View Online

Vertically cross-linking silver nanoplate arrays with controllable density based on seed-assisted electrochemical growth and their structurally enhanced SERS activity†

Guangqiang Liu, Weiping Cai,* Lingce Kong, Guotao Duan and Fangjing Lü

Received 19th August 2009, Accepted 21st October 2009
First published as an Advance Article on the web 24th November 2009
DOI: 10.1039/b917167c

Downloaded by Hefei Institutes of Physical Science, Chinese Academy of Sciences on 04 March 2011
Published on 24 November 2009 on http://pubs.rsc.org | doi:10.1039/B917167C

A facile seed-assisted electrochemical deposition (ECD) route has been presented to fabricate silver nanoplate arrays at room temperature. The nanoplates are hundreds of nanometres to several micrometres in dimension and tens of nanometres in thickness. All the nanoplates are standing vertically on the indium-tin oxide substrate and cross-linking each other. Importantly, the number density of silver nanoplates in the array can be controlled by the amount of seeds pre-coated on the substrate. Further experiments have demonstrated that electric current density during ECD plays a crucial role in the final morphology of the products. A simple and flexible way is presented to study time-dependent morphological evolution only in one step, based on substrate-moved electrochemical deposition, which has revealed that each nanoplate grows up from individual Ag seeds on the substrate. The formation of nanoplates is attributed to the seed-assisted preferential nucleation and quasi-equilibrium oriented growth. Further studies indicate that such Ag nanostructured arrays can serve as highly active surface-enhanced Raman scattering (SERS) substrates and have very homogeneous SERS activity in whole sample.

1. Introduction

Metal micro- and nano-structures have attracted significant attention due to their widespread application in optics, electronics, optoelectronics, information storage, catalysis, biological and chemical sensing, and surface-enhanced Raman scattering (SERS).[1] Silver nanoplates, particularly, have been intensively studied because of the strong relation between their shape and the optical properties. For example, triangular silver nanoplates show ample surface plasmon resonance (SPR) properties compared to spherical silver nanoparticles.[2] The strong SPR peak of the in-plane dipole resonance of the silver nanoplates can be easily tuned from the visible to the near-infrared (IR) region of the spectrum, depending on the shape and size.[3] A few methods have been developed for synthesizing silver nanoplates, including photochemistry,[4] thermo-chemistry,[5]wet-chemistry,[6]and biochemistry.[7] In most of these methods, Ag nanoplates are dispersed in solution, which restricts the application of nanoplates in some cases. Fabrication of some nano-devices often needs assembly of these Ag nano-objects on the substrates directly.[8] At present, the direct growth of Ag or Au nanoplates on substrates with a controllable pattern is a hot topic. For example, Umar and Uyama reported the formation of gold nanoplates layed on indium tin oxide (ITO) through a liquid-phase reduction method.[9] Sun and Wiederrecht demonstrated a simple and surfactant-free approach to fast produce pristine metal nanoplates with well-controlled thicknesses through a galvanic reaction.[10] Recently, we adopted an electrochemical-deposition method to fabricate trapeziform-like Ag nanosheet arrays standing on Au/Si substrates.[11] These nanoplates were all standing on the substrates separately, however, the number density of nanosheets standing on the substrates can not be controlled, which is disadvantageous for some applications, for example SERS.

Here, we report a simple approach to fabricate silver nanoplate arrays, with controllable distribution densities, on an ITO substrate based on seed-assisted electrochemical growth. The electrochemical deposition was conducted on the ITO substrate pre-coated with Ag-seeds, under a low current density at room temperature, so that the nanoplates nucleate preferentially on the seeds. It has been shown that the prepared nanoplates are standing nearly vertically on the substrate and cross-linking together. The number density of Ag nanoplates can be controlled by the amount of Ag-seeds on the ITO substrate. This cross-linking nanoplate array with a controllable number density has exhibited a highly active SERS effect and very homogeneous SERS activity in the whole sample, since there are many edges or controlled nano-gaps in the uniform array, which can serve as "hot sites" for the local surface plasmon resonance enhancement.[12] Also, this array could be of potential application in a fuel encapsulation cell as a catalyst due to its high specific surface area.[13] The details are reported in this article.

2. Experiment section

2.1. Pre-coating of Ag-seeds on substrates

Silver colloidal solution was first prepared. Typically, 0.5 mL of 60 mM $AgNO_3$ and 1 mL of 35 mM sodium citrate were added to 98 mL of water. The mixed solution was stirred for several

Key Lab of Materials Physics, Anhui Key Lab of Nanomaterials and Nanotechnology, Institute of Solid State Physics, Chinese Academy of Sciences, Hefei 230031, P.R. China. E-mail: wpcai@issp.ac.cn

† Electronic supplementary information (ESI) available: Further characterisation and estimation of enhancement factor. See DOI: 10.1039/b917167c

View Online

Downloaded by Hefei Institutes of Physical Science, Chinese Academy of Sciences on 04 March 2011
Published on 24 November 2009 on http://pubs.rsc.org | doi:10.1039/B917167C

minutes. Then, 0.5 mL of an aqueous 20 mM $NaBH_4$ solution, which had been aged at room temperature for 2 h, was added quickly, stirred for 1 h and then aged at room temperature for 24 h before use. ITO substrates (1 × 2 cm^2) were ultrasonically cleaned in acetone and then in ethanol for 1 h, respectively. A droplet of the prepared Ag colloidal solution (100 μL) was spin-coated on the cleaned substrate on a custom-built spin coater. The coating area on the substrate was fixed to be about 1 cm in diameter. After that, the substrate was dried at 40 °C.

2.2. Electrochemical deposition

Electrolyte solution was prepared by adding 0.05 g $AgNO_3$ and 0.25 g PVP to 50 ml of water and then stirring until complete dissolution. The electrochemical deposition was carried out under galvanostatic conditions at a low current density of 5 μA cm^{-2} at room temperature on a domestic electrochemical device (Shanghai Precision & Scientific Instrument Company, model DJS-292). A graphite flake was used as the anode and the Ag seed-coated ITO substrate as cathode. After deposition for about 10 h, the substrate with products was taken out, cleaned with distilled water several times and dried with high-purity flowing nitrogen for characterization and property studies.

2.3. Characterization

The as-prepared samples were characterized by X-ray diffraction (XRD) (Philips X'pert-PRO, Cu Kα (0.15418 nm) radiation), field emission scanning electronic microscopy (FESEM) (Sirion 200 FEG). For transmission electron microscopy (TEM) (JEOL 2010, at 200 kV) examination, the products were scraped off from the ITO substrate and dispersed in ethanol by ultrasonication. Before Raman spectral measurements, the samples were immersed in 10^{-6} mol L^{-1} rhodamine 6G (R6G) or 4-aminothiophenol (4-ATP) solution for 30 min, rinsed with de-ionized water, and dried with high-purity flowing nitrogen. The Raman spectra were recorded on a macroscopic confocal Raman spectrometer, using a laser beam with an excitation wavelength of 514 nm. The data integration time was 3 s for all samples.

3. Results and discussion

3.1. Morphology and structure

Ag seeds in the pre-prepared colloidal solution are nearly spherical in shape and fall into the range 5 nm to 30 nm in size [most (80%) Ag seeds were 15–20 nm in size], as shown in Figure S1 (ESI†). The optical absorbance spectrum of the colloidal solution shows a strong absorption peak at 390 nm, corresponding to the surface plasmon resonance of the Ag nanoparticles, as illustrated in Fig. S2 (ESI†). After electrodeposition on the ITO substrate coated with the Ag-seeds, the Ag nanoplate arrays were obtained, as typically illustrated in Fig. 1a. We can see that the products consist of nanoplates. The number density is about 1.2 × 10^8 plates cm^{-2}. Almost all the nanoplates are cross-linked together and stand nearly vertical on the substrate. Local magnification has revealed that the nanoplates are about 50 nm in thickness, as shown in Fig. 1b. Obviously, there are many nano-gaps formed among the interlaced nanoplates.

The corresponding XRD pattern shows four diffraction peaks (2θ) at 38.2, 44.3, 64.4, and 77.3°, corresponding to the (111),

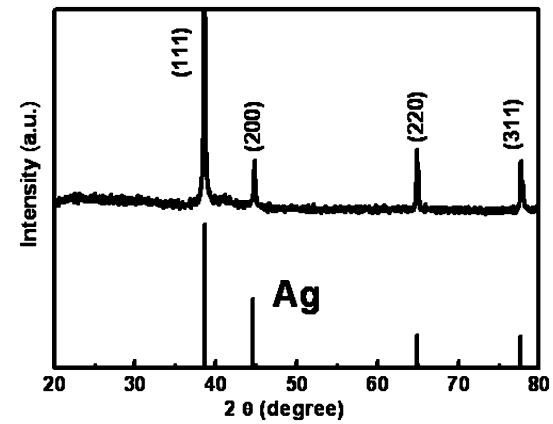

Fig. 2 XRD of the as-prepared sample shown in Fig. 1. The lower line-spectrum is the standard diffraction of Ag powders.

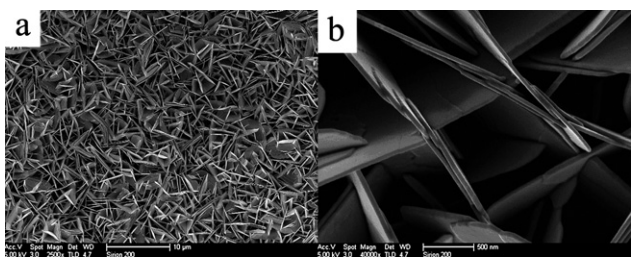

Fig. 1 FESEM image of the as-prepared products on the Ag seed-coated ITO substrate under a deposition current 5μA cm^{-2} (see the text). (a) Low magnification, (b) the local magnification of (a).

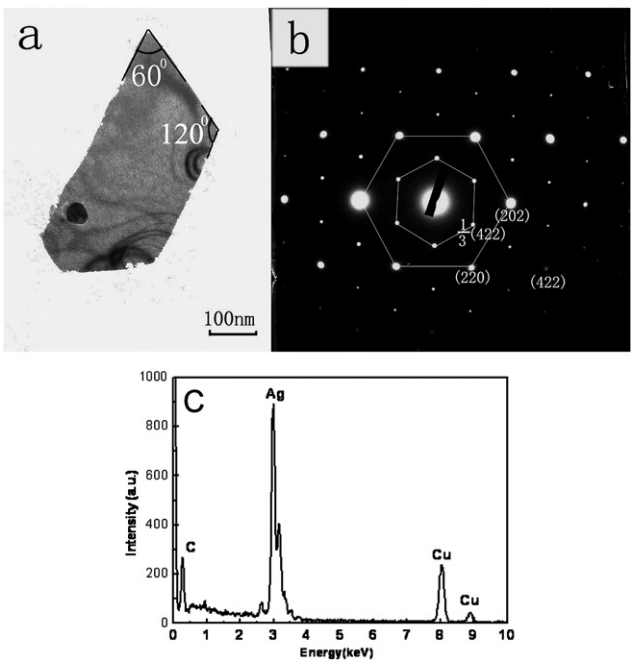

Fig. 3 TEM image (a) and corresponding electron diffraction pattern (b) of a single Ag nanoplate lying on a TEM grid; (c) EDX spectrum of the as-prepared sample shown in Fig. 1.

 This journal is © The Royal Society of Chemistry 2010

View Online

Downloaded by Hefei Institutes of Physical Science, Chinese Academy of Sciences on 04 March 2011
Published on 24 November 2009 on http://pubs.rsc.org | doi:10.1039/B917167C

(200), (220), and (311) planes, respectively, of the face-centered cubic (*fcc*) structure of silver with the space group *Fm3m* (JCPDS), as shown in Fig. 2. The intensity ratio of the {111} to {200} diffraction peaks in the XRD spectrum is much higher than that of bulk (about 2). This indicates that the as-prepared nanoplates are abundant in the {111} planes.

Further, TEM examination was conducted. Fig. 3a presents a typical TEM image for a single nanoplate. The nanoplate is polygonal and its base surface is smooth. Two adjacent edges tend to form angles of 60° or 120°. Fig. 3b shows the selected area electron diffraction (SAED) pattern by directing the electron beam perpendicular to the base face of the nanoplate. The inner set of spots is believed to originate from the $\frac{1}{3}$ {422} planes normally forbidden by an *fcc* lattice. According to the results of Mirkin and coworkers,[14] such $\frac{1}{3}$ {422} forbidden reflections observed on the plate-like structures of silver or gold should be attributed to {111} stacking faults parallel to the {111} surface and extending across the entire nanoplates. The second set of spots were indexed to {220} Bragg reflections, which indicate that the as prepared nanoplates are single-crystalline with {111} lattice planes as the basal planes and <110> as the edges. The composition has also been analyzed by energy-dispersive X-ray spectroscopy, as shown in Fig. 3c. There are only the peaks for Ag, Cu and C. Herein, Cu and C are from TEM grid, which demonstrates that the samples are of high purity.

3.2. Influence of deposition conditions

Further experiments have revealed that many factors influence the formation of the nanoplate arrays, such as, deposition current density, deposition time, and amount of Ag seeds on the substrate.

3.2.1. Deposition current density. High current density is not beneficial for the formation of nanoplate arrays. When the current density is increased to 20 μA cm^{-2}, the products were mixed with large particles and the nanoplates, as shown in Fig. 4a. If the current density was increased to a very high value (say, 50μA cm^{-2}), the final product was dominated by large Ag particles together with only a few nanoplates (see Fig. 4b). Only at a low current density (≤5 μA cm^{-2}), can we obtain the nanoplate arrays.

3.2.2. Deposition time. Morphological evolution of the Ag nanoplate arrays during electric-deposition was examined. Usually it needs a series of experiments with different deposition times to get the results of morphological evolution with deposition time, and hence it is time-consuming. Here, we have designed a simple and flexible way to obtain such results of the morphological evolution only in one step based on substrate-moved electrochemical deposition, as schematically shown in

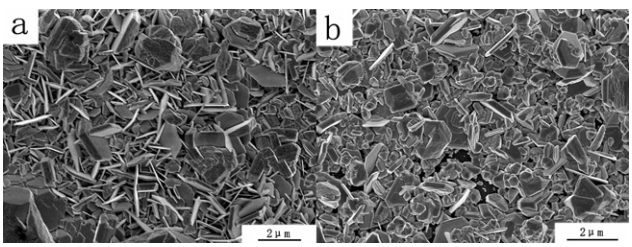

Fig. 4 FESEM images of the samples prepared at higher deposition current densities. (a) 20μA cm^{-2}, (b) 50μA cm^{-2}.

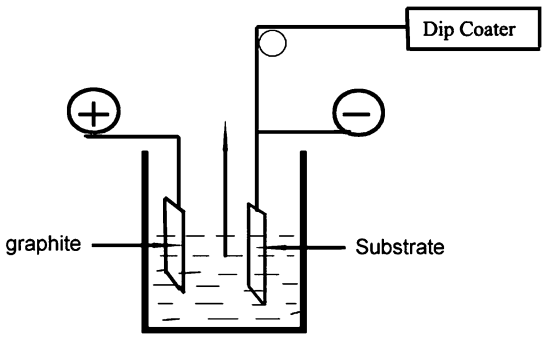

Scheme 1 The schematic illustration of cathode-moved electrochemical deposition controlled by a step mortar.

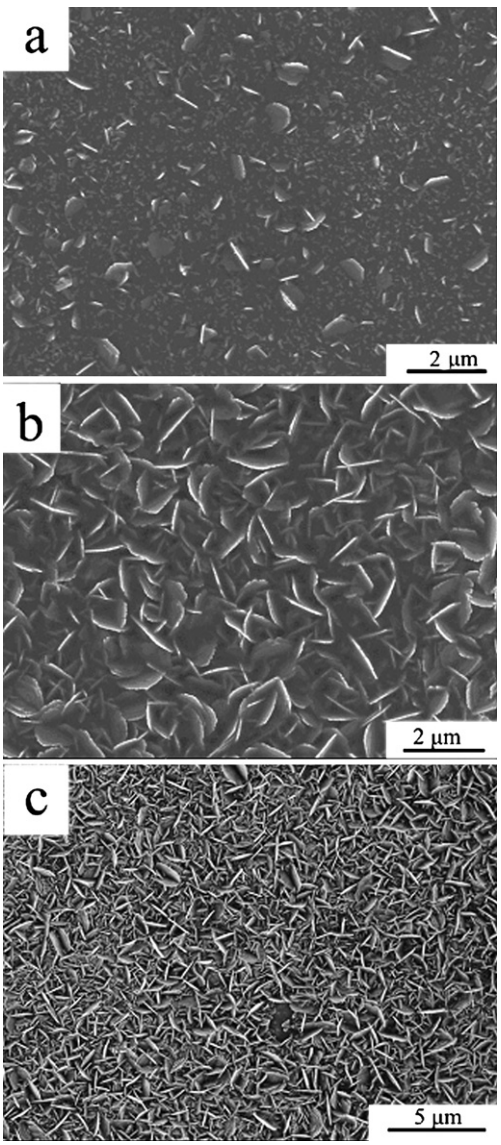

Fig. 5 FESEM images of Ag nanostructures after deposition for different time through a cathode-moved electrochemical deposition experiment. (a) 10 min; (b) 1 h; (c) 5 h.

View Online

Downloaded by Hefei Institutes of Physical Science, Chinese Academy of Sciences on 04 March 2011
Published on 24 November 2009 on http://pubs.rsc.org | doi:10.1039/B917167C

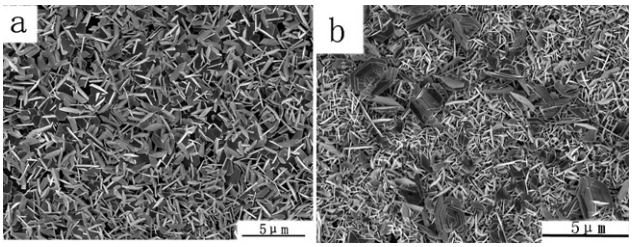

Fig. 6 FESEM images of the samples prepared on ITO coated with (a) 50 μL and (b) 150 μL Ag colloidal solution (deposition current density: 5 μA cm^{-2}) (see the text).

Scheme 1. The substrate was ever-moving very slowly (about 0.25 μm s^{-1}) vertically out of the surface of electrolyte solution during deposition. The morphological evolution can thus be observed in one substrate from its upper to lower parts. Fig. 5 shows the morphologies from different parts of the substrate, corresponding to different deposition times. When the deposition time is short (say, 10 min), only a few small nanoplates are observed and nearly vertically stand on the seed-coated substrate (Fig. 5a). The longer deposition time leads to the growth of the nanoplates and more nanoplates can be observed. When the time reaches about 1 h, the observed number density of nanoplates significantly increases and the nanoplates are about one micrometre in planar dimension, but very thin in thickness (Fig. 5b). If the deposition time is further increased, the vertically standing Ag nanoplates are denser in distribution and ever-increased in size (Fig. 5c). In addition, such substrate-moved deposition is very time-saving, and we can get time-dependent morphological evolution of the nanosheets in one step.

3.2.3. Amount of seeds. The amount of Ag seeds on the ITO substrate is also crucial to the distribution density of Ag nanoplates. For the ITO substrate without coating, we cannot get any Ag product on the ITO substrate at a low current density (5 μA cm^{-2}). If we coat the substrate with only a droplet (50 μL) of the Ag colloidal solution (keeping the same coated area as the sample above, the diameter is 1 cm), the number density of the nanoplates is about 8.0×10^7 plates cm^{-2} (see Fig. 6a), lower than that shown in Fig. 1a. The higher amount of Ag seeds corresponds to the higher distribution density of nanoplates on the substrate. Fig. 6b corresponds with the result from the substrate coated with a droplet of 150 μL Ag colloidal solution, and the number density is estimated to be about 3.0×10^8 plates cm^{-2}. These indicate the controllability of the distribution density by an amount of the Ag seeds on the substrate, which is important in the fabrication of nanodevices.

3.3. Formation of nanoplate arrays

Under an electric field, the Ag^+ in the electrolyte will move to the surface of the cathode and the reduction reaction take place:

$$Ag^+ + e \rightarrow Ag^\circ \quad (1)$$

The reduced Ag° atoms will nucleate on the random-oriented Ag seeds because of the low nucleation energy. The nucleation could preferentially take place on some Ag seeds with {110} surface plane because of the high surface energy [$\gamma_{(110)} > \gamma_{(100)} > \gamma_{(111)}$].[13] The formed nuclei will grow with the terminal planes {111}, with the lowest surface energy, according to a quasi-equilibrium growth mode due to low current density. Finally, the nanoplates are formed, as illustrated in Scheme 2. Obviously, when a nanoplate is standing on the substrate surface, and especially, perpendicular to the substrate, it will grow up more easily. Otherwise, if it is parallel to the substrate surface, it can not grow because of the space limitation. Also, when the nanoplates are very dense, they will jostle each other and form cross-linking structures nearly vertically standing on the substrate. Growth of the nanoplates from the seeds on the

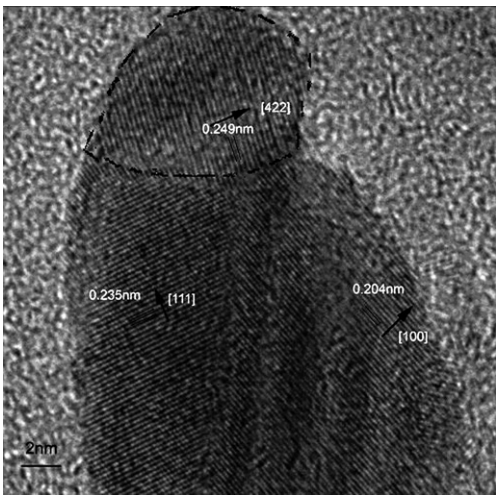

Fig. 7 High resolution TEM image of a single particle in the sample obtained after electrochemical deposition for 30 min.

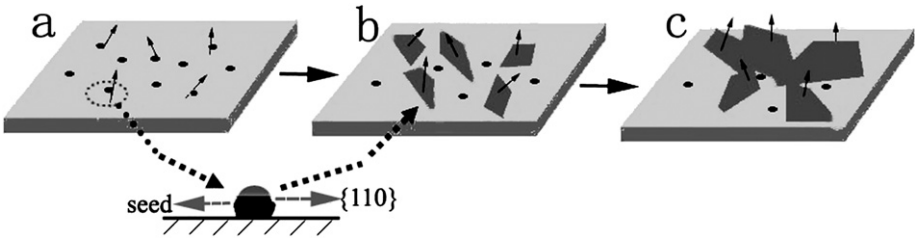

Scheme 2 A schematic illustration of the preferential nucleation and oriented growth for cross-linking Ag nanoplate arrays: (a) random-oriented Ag seeds laying on the ITO substrate, and Ag nuclei are preferentially formed on some <110>-oriented seeds (see arrow's marks); (b) oriented growth of the nuclei along the fastest <110> within {111} plane under a low deposition current density; (c) cross-linking Ag nanoplate array structure is formed and standing on the substrate vertically.

 This journal is © The Royal Society of Chemistry 2010

View Online

Downloaded by Hefei Institutes of Physical Science, Chinese Academy of Sciences on 04 March 2011
Published on 24 November 2009 on http://pubs.rsc.org | doi:10.1039/B917167C

substrate has been confirmed by high resolution TEM examination, as illustrated in Fig. 7, corresponding to a single nanoparticles in the sample obtained after electrochemical deposition for only 30 min. The top part of the particle should correspond to an initial growing nanoplate. The fringe spacing with 0.249 nm is observed, which is close to 1/3 *d*-value of the (422) reflection of Ag. This plane can be found only in the nanoplates of the noble metal with *fcc*. The bottom part of the particle corresponds to one Ag seed on the substrate. Obviously, the small nanoplate starts growing on the seeds.

On the basis of the discussion above, the influence factors for morphology of products are easily understood. The more Ag seeds correspond to formation of more nuclei and the denser distribution of the final formed nanoplates. Under a high current density, deposition rate will be fast and hence quasi-equilibrium growth can not take place. We can not obtain the nanoplate arrays (Fig. 4b).

3.4. SERS measurements

Zhang *et al.*[15] found that silver nanoplates, prepared by a solution-based solvothermal method and lying on a substrate, possessed the poorest SERS activity compared to silver nanoparticles and nanowires on the substrate. It meant that Ag nanoplates are unfavorable for SERS in that case. However, when the nanoplates stand vertically on the substrate and form the array with a high distribution density or high density of nanogaps, as presented in this study, the situation should be different. This has been confirmed by our experiments, as shown in Fig. 8, corresponding to the Raman spectra of R6G on the Ag nanoplate arrays (after immersion in 10^{-6} mol L^{-1} R6G solution for 30 min). Our nanoplate arrays show much higher SERS activity than the normal Ag particles film synthesized by the usual mirror reaction (the morphology and preparation details are seen in Fig. S3, ESI† and its caption, respectively), and hence are highly active SERS substrates. Further, the SERS activity rises with the increase of the distribution density of the nanoplates in the arrays in this study (see curves 2–4 in Fig. 8).

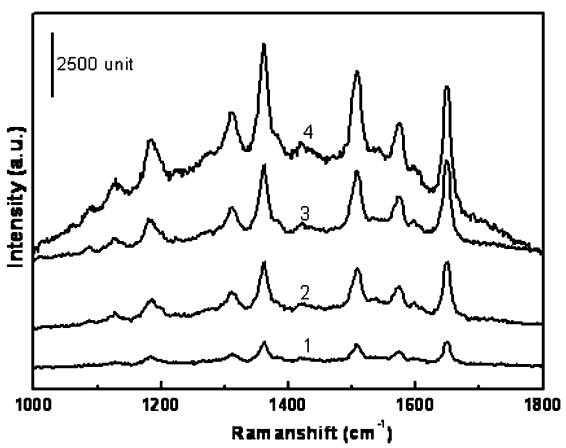

Fig. 8 Raman spectra of R6G on different substrates after immersion in 10^{-6} mol L^{-1} R6G solution for 30 min. Curve 1: Ag nanoparticle film obtained by usual mirror reaction; curves 2–4: Ag nanoplate arrays on the ITO substrates coated with 50 μL, 100 μL and 150 μL Ag colloidal solutions, respectively.

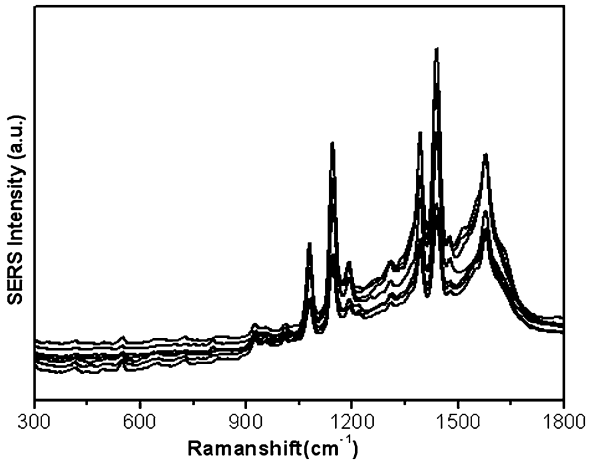

Fig. 9 Raman spectra of 4-ATP from seven different spots on the fabricated vertically cross-linking silver nanoplate array shown in Fig. 1.

Taking 4-aminothiophenol (4-ATP) as test molecules, the enhancement factor (EF) of the samples was estimated, in order of magnitude, by the equation:

$$EF = (I_{SERS}/N_{ads})/(I_{bulk}/N_{bulk}) \quad (2)$$

where I_{SERS} and I_{bulk} are the Raman signals at a representative vibration (1075 cm^{-1} in our case) for the 4-ATP molecules adsorbed on a substrate with SERS effect and solid 4-ATP, respectively. N_{ads} and N_{bulk} are the numbers of the adsorbed molecules and the solid 4-ATP within the laser spot, respectively. We can thus obtain the EF values 5×10^3 for the Ag nanoparticle film, prepared by usual mirror reaction, and $>2 \times 10^5$ for the Ag nanoplate arrays (the details of estimation can be seen in "Estimation of enhancement factor" and Fig. S4 in the ESI†). The enhancement effect of the latter is much higher (two orders of magnitude) than that of the former.

Further measurements have revealed that the reproducibility of the SERS signal at different spots on the fabricated silver nanoplate arrays is very good. Fig. 9 shows the Raman spectra of 4-aminothiophenol (4-ATP) on the sample, collected at random seven spots, exhibiting the good measurement reproducibility across the whole substrate. This is attributed to the highly homogeneous structure of such arrays.

It is well known that SERS is a very local phenomenon occurring at crevices or in pores of the rough surface.[16] In our case, the high SERS activity can be attributed to the following two points. (i) The as-prepared arrays are very uniform, which is an important for SERS,[17] and importantly, the nanoplates stand nearly vertically on the substrate, forming cross linking-like arrays with high specific surface area, which favors the adsorption of probing molecules. (ii) The high density of interstitials or nanogaps is formed among the nanoplates, which provides many "hot spots".[18] Obviously, the higher distribution density of the nanoplates corresponds to more "hot spots", leading to an ever-increasing SERS activity with the distribution density of the nanoplates (see curves 2–4 in Fig. 8).

In addition, the intensity of the SERS signal for the arrays exhibits dependence on the incident angle of the excited laser beam. For instance, when the incident angle is 10° (relative to the

View Online

Downloaded by Hefei Institutes of Physical Science, Chinese Academy of Sciences on 04 March 2011
Published on 24 November 2009 on http://pubs.rsc.org | doi:10.1039/B917167C

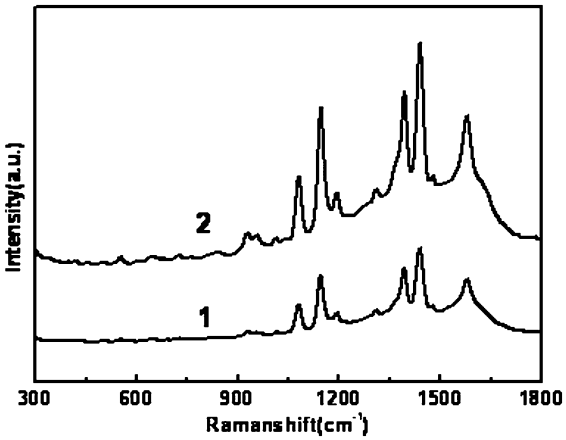

Fig. 10 Raman spectra of the 4-ATP on the vertically cross-linking silver nanoplate array, shown in Fig. 1, with different incident directions of laser beam. Curve 1: vertical incident direction, and curve 2: slanted incident direction (about 10° relative to vertical incident direction).

normal direction), the Raman signal is much stronger than that of the normal measurement, as illustrated in Fig. 10. Such signal enhancement is attributed to the unique structure of the vertically standing nanoplate array. Slanted incidence can excite the more molecules absorbed on side surface of nanoplates. This means that the structure of vertically standing and cross-linking nanoplate arrays leads to not only more "hot spots" but also adsorption of more probing molecules, and slanted excitation can get a much stronger detection signal, which is important for the design of SERS devices based on such arrays.

4. Conclusion

In summary, cross-linking Ag nanoplate arrays have been successfully synthesized on the seed-coated ITO substrate by a simple and convenient electrochemical deposition at a low current density. We can control the distribution density of Ag nanoplates by the amount of seeds coated on the ITO substrate. The formation of nanoplates can be attributed to seed-assisted nucleation and quasi-equilibrium preferential growth. Such Ag nanoplate arrays show high SERS activity with high signal reproducibility and hence are good candidates for the highly active SERS substrates. In addition, this study could be important for us to vertically immobilize Ag nanoplates on a solid substrate, which is beneficial to fabrication of the nanodevices for some purposes.

Acknowledgements

This work is financially supported by Natural Science Foundation of China (Grant No. 50831005 and 10704075), and the Major State research program of China "Fundamental Investigation on Micro-Nano Sensors and Systems based on BNI Fusion" (Grant No. 2006CB300402).

Reference and Notes

1 (*a*) W. Fritzsche and T. A. Taton, *Nanotechnology*, 2003, **14**, R63; (*b*) N. R. Jana, L. Gearheart, S. O. Obare and C. J. Murphy, *Langmuir*, 2002, **18**, 922; (*c*) C. Salzemann, I. Lisiecki, A. Brioude, J. Urban and M. P. Pileni, *J. Phys. Chem. B*, 2004, **108**, 13242; (*d*) S. H. Sun, C. B. Murray, D. Weller, L. Folks and A. Moser, *Science*, 2000, **287**, 1989; (*e*) N. I. Kovtyukhova and T. E. Mallouk, *Chem.–Eur. J.*, 2002, **8**, 4354; (*f*) A. Tao, F. Kim, C. Hess, J. Goldberger, R. G. He, Y. G. Sun, Y. N. Xia and P. D. Yang, *Nano Lett.*, 2003, **3**, 1229.
2 Y. G. Sun, B. T. Mayers and Y. N. Xia, *Nano Lett.*, 2003, **3**, 675.
3 X. Q. Zou and S. J. Dong, *J. Phys. Chem. B*, 2006, **110**, 21545.
4 (*a*) R. C. Jin, Y. W. Cao, E. Hao, G. S. Métraux, G. C. Schatz and C. A. Mirkin, *Nature*, 2003, **425**, 487–490; (*b*) M. Maillard, P. Huang and L. Brus, *Nano Lett.*, 2003, **3**, 1611; (*c*) Y. Zhou, C. Y. Wang, Y. R. Zhu and Z. Y. Chen, *Chem. Mater.*, 1999, **11**, 2310.
5 (*a*) Z. Li, Z. Liu, J. Zhang, B. Han, J. Du, Y. Gao and T. Jiang, *J. Phys. Chem. B*, 2005, **109**, 14445; (*b*) I. Pastoriza-Santos and L. M. Liz-Marzan, *Nano Lett.*, 2002, **2**, 903; (*c*) G. S. Métraux and C. A. Mirkin, *Adv. Mater.*, 2005, **17**, 412.
6 (*a*) J. E. Millstone, S. Park, K. L. Shuford, L. D. Qin, G. C. Schatz and C. A. Mirkin, *J. Am. Chem. Soc.*, 2005, **127**, 5312; (*b*) T. K. Sau and C. J. Murphy, *J. Am. Chem. Soc.*, 2004, **126**, 8648; (*c*) N. Malikova, I. Pastoriza-Santos, M. Schierhorn, N. A. Kotov and L. M. Liz-Marzán, *Langmuir*, 2002, **18**, 3694.
7 (*a*) S. S. Shankar, A. Rai, B. Ankamwar, A. Singh, A. Ahmad and M. Sastry, *Nat. Mater.*, 2004, **3**, 482; (*b*) S. S. Shankar, A. Rai, A. Ahmad and M. Sastry, *Chem. Mater.*, 2005, **17**, 566; (*c*) R. R. Naik, S. J. Stringer, G. Agarwal, S. E. Jones and M. O. Stone, *Nat. Mater.*, 2002, **1**, 169; (*d*) B. Liu, J. Xie, J. Y. Lee, Y. P. Ting and J. P. Chen, *J. Phys. Chem. B*, 2005, **109**, 15256.
8 X. J. Huang, A. M. O'Mahony and R. G. Compton, *Small*, 2009, **5**, 776.
9 A. A. Umar and M. Oyama, *Cryst. Growth Des.*, 2006, **6**, 818.
10 Y. G. Sun and G. P. Wiederrecht, *Small*, 2007, **3**, 1964.
11 G. Q. Liu, W. P. Cai and C. H. Liang, *Cryst. Growth. Des*, 2008, **8**, 2748.
12 J. T. Zhang, X. L. Li, X. M. Sun and Y. D. Li, *J. Phys. Chem. B*, 2005, **109**, 12544.
13 (*a*) C. W. Xu, H. Wang, P. K. Shen and S. P. Jiang, *Adv. Mater.*, 2007, **19**, 4256; (*b*) G. Chang, J. D. Zhang, M. Oyama and K. Hirao, *J. Phys. Chem. B*, 2005, **109**, 1204.
14 R. C. Jin, Y. W. Cao, C. A. Mirkin, K. L. Kelly, George C. Schatz and J. G. Zheng, *Science*, 2001, **294**, 1901.
15 J. Zhang, X. Li, X. Sun and Y. J. Li, *J. Phys. Chem. B.*, 2005, **109**, 12544.
16 (*a*) M. Suzuki, Y. Niidome, Y. Kuwahara, N. Terasaki, K. Inoue and S. Yamada, *J. Phys. Chem. B*, 2004, **108**, 11660; (*b*) G. T. Duan, W. P. Cai, Y. Y. Luo, Y. Li and Y. Lei, *Appl. Phys. Lett.*, 2006, **89**, 211905.
17 (*a*) G. T. Duan, W. P. Cai, Y. Y. Luo, Y. Li and Y. Lei, *Appl. Phys. Lett.*, 2006, **89**, 181918; (*b*) V. S. Zuev, A. V. Frantsesson, J. Gao and J. G. Eden, *J. Chem. Phys.*, 2005, **122**, 214726.
18 (*a*) H. H. Wang, C. Y. Liu, S. B. Wu, N. W. Liu, C. Y. Peng, T. H. Chan, C. F. Hsu, J. K. Wang and Y. L. Wang, *Adv. Mater.*, 2006, **18**, 491; (*b*) S. J. Lee, A. R. Morrill and M. Moskovits, *J. Am. Chem. Soc.*, 2006, **128**, 2200.

 This journal is © The Royal Society of Chemistry 2010